Mn^{2+} as a Radial Pressure Gauge in Colloidal Core/Shell Nanocrystals

Sandrine Ithurria,[1] Philippe Guyot-Sionnest,[2] Benoit Mahler,[1] and Benoit Dubertret[1]

[1]*Laboratoire Photons Et Matière, UPR5 du CNRS, ESPCI 10 rue Vauquelin, 75231 Paris, France*

[2]*James Franck Institute, The University of Chicago, Chicago, Illinois 60637 USA*

(Received 31 July 2007; published 27 December 2007)

The fluorescence of Mn^{2+} doped in the shell of CdS/ZnS core/shell nanocrystals at radially controlled position is used as a local probe of pressure in the nanocrystal shell. The redshift of the fluorescence with increasing shell thickness indicates a pressure of more than 4 GPa for 7.5 monolayers of ZnS. The radial dependence and magnitude of the pressure derived from the Mn^{2+} fluorescence shift are in good agreement with the spherically symmetric elastic continuum model and the 7% misfit between the core and the epitaxial shell.

DOI: 10.1103/PhysRevLett.99.265501 PACS numbers: 61.46.Df, 71.20.Nr, 71.55.Gs, 73.21.La

Colloidal semiconductor Quantum Dots (QD) are a growing class of materials which offer tunable optical and electronic properties [1]. In particular, luminescent and stable core/shell nanocrystals, such as CdSe/ZnS [2] and other combinations, have facilitated the multifaceted applications of these materials. While lattice mismatch and band offsets have provided a rough design guideline for colloidal heterostructures, there has been little discussion of strain, unlike for planar heterostructures which have long been studied [3]. In principle, the finite interfacial area of nanostructures guarantees that lattice mismatch can be accommodated; however, strain may still be large enough to generate dislocations. For example, a few ZnS layers can be grown epitaxially on CdSe nanocrystals, but defects are introduced when more ZnS is deposited [4]. Understanding the physical consequences of lattice mismatch may help in designing better core/shell structures. Yet, local strain within colloidal nanostructures has not been measured because of the lack of appropriate technique. High resolution Transmission Electron Microscopy (TEM) can hardly resolve local lattice changes of a few percent, while x-ray diffraction only provides volume averaged values. In this Letter, in analogy with the Ruby fluorescence used in high pressure experiments [5], the fluorescence of the Mn^{2+} dopant placed at a well defined position in a core/shell system provides a first view of the radial pressure distribution. The observations are then validated by the predictions of a simple elastic continuum model.

The system studied is the CdS/ZnS core/shell nanocrystals where the Mn^{2+} radial position is precisely controlled within the shell, a system recently developed by Cao and co-workers [6]. All samples used the same CdS cores [7] that were grown for 10 min. at 240 °C. The cores have a narrow exciton emission peak at ~420 nm and a zinc-blend crystal structure. Their diameter is ~3.3 nm using the relations established by Peng and co-workers [8]. The ZnS shell was grown monolayer by monolayer (ML), by alternate injections of Zinc-stearate solution (0.1*M*) in octadecene (ODE) and sulfur in ODE (0.1*M*) in a reaction mixture with the host particle (CdS or CdS/ZnS) dispersed in 3.6 ml of ODE and 1.2 ml of Oleylamine. One monolayer is taken to correspond to a radius increase of $a/2$ where a is the lattice constant of ZnS ($a = 0.542$ nm). The synthesis consists of first the growth of x ML of ZnS. Then, Mn^{2+} is incorporated by injecting 0.28 ml of a Manganese acetate solution in Oleylamine (0.5 m*M*). The amount is equivalent to 13 atoms of manganese per dots. However, the insertion yield is only 30% so that there should be about 4 Mn^{2+} per nanoparticles [6]. The particles are then precipitated to eliminate unreacted Mn precursors. Afterwards, the dots are added to a growth mixture to finish the deposition of the 7 ML of ZnS. A final injection of Zinc-stearate provides the last $\frac{1}{2}$ ML. The samples are indexed by the number of ZnS ML between Mn^{2+} and the CdS cores, varying from 0 to 6, corresponding to a Mn^{2+} radial position varying between 1.65 and 3.3 nm.

Aliquots were extracted from the reaction mixture after each ZnS layer over the Mn^{2+} layer. TEM confirmed the increase radii as the layers are deposited. The final dots are rather spherical with a diameter very close to the expected 7.45 nm. They remain monodispersed (<10%) with a narrow photoluminescence from the CdS, ~19 nm full-width half maximum, and single crystalline as shown in Fig. 1. UV-visible absorption and fluorescence excitation spectra also show the increasing contribution from the ZnS absorption. The Electron Paramagnetic Resonance (EPR) of the Mn^{2+} ions confirmed the tetrahedral bonding of Mn^{2+}. There is a small systematic increase of the hyperfine splitting from $A_{iso} \approx (68.3 \pm 0.05) \times 10^{-4}$ cm^{-1} to $A_{iso} \approx (68.5 \pm 0.05) \times 10^{-4}$ cm^{-1} from 0 to 6 ML, respectively. The EPR spectrum shows narrow hyperfine lines and no broad background which would be due to Mn-Mn interactions, confirming that the Mn is dilute [9].

The main result analyzed here is the smooth shift of the Mn^{2+} PL as more ZnS layers are deposited. For the 0 ML sample where Mn^{2+} is at the CdS/ZnS interface, the Mn^{2+} PL peak varies incrementally from ~2.09 to 1.96 eV as the ZnS shell increases to 7.5 ML. Similarly, for the fixed

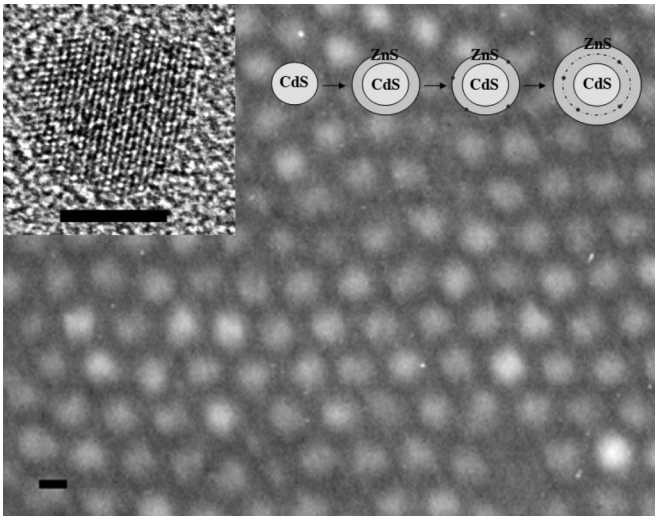

FIG. 1. TEM image of the $CdS/ZnS_{7.5\ ML}$ doped with manganese. The inset shows the lattice resolution throughout the nanocrystal. The scale bar is 5 nm. The growth scheme is shown.

7.5 ML ZnS shell, the Mn^{2+} PL peak tunes strongly with depth, from 2.11 to 1.96 eV for the 6 to the 0 ML samples, respectively. The normalized Mn^{2+} PL at the different depths are shown in Fig. 2.

Figure 3(a) shows the Mn^{2+} PL peak values for the seven radial positions of the Mn^{2+} ions, as a function of shell thickness. There is a systematic trend in these data, where more overlayers of ZnS lead to a redder emission and where the tuning is largest as the Mn^{2+} is closer to the interface. In the bulk, Mn^{2+} fluoresces orange, and the most documented value given for ZnS is 2.12 eV [10]. The peak emission of Mn^{2+} is however sensitive to the next nearest neighbors and the distortion from the tetrahedral sites. It could therefore be that each of the different values

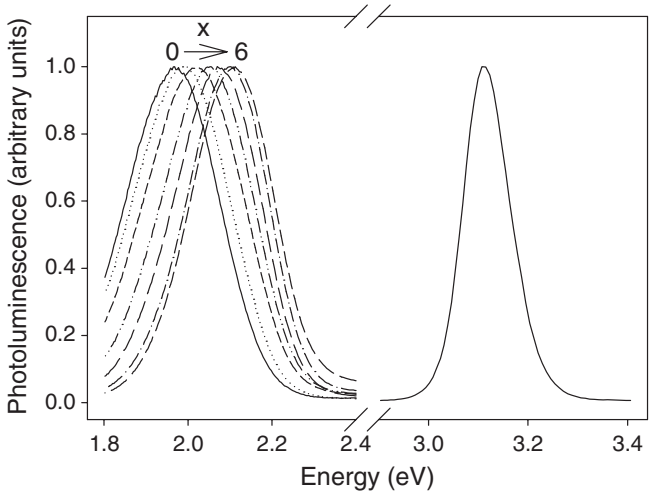

FIG. 2. Left: blueshift of the Mn^{2+} PL for $CdS/ZnS_{xML}/Mn/ZnS_{(7.5-x)ML}$ with x increasing from 0 to 6. Right: emission of undoped CdS/ZnS(7.5 ML).

measured corresponds to small differences in local environment.

On the other hand, it seems likely that after the first ML of ZnS is deposited on the Mn^{2+}, the local environment is set, and that the tuning with thicker overlayers reflects a longer range effect, of which pressure is a likely candidate. In bulk ZnS, the Mn^{2+} emission tunes with pressure at a rate $\alpha \sim -30.4$ meV/GPa [11]. The redshift of 127 meV observed here for the 0 ML sample as the ZnS shell increases from 1 to 7.5 ML, and therefore corresponds to a very large pressure increase of 4.2 GPa.

Surface tension in spherical particles gives rise to the Laplace pressure $P = 2\gamma/R$, where R is the particle radius and γ is the surface tension. For the ZnS surface passivated with the organic ligands, γ is not known. However, for CdSe nanocrystals also passivated but with different organic ligands, a size-dependent γ was reported as $\gamma = 0.34 + 0.84/R^2$ (nm) N/m [12]. Using this value as a guideline, the Laplace pressure *decreases* by 0.3 GPa as the ZnS shell increases from 1 to 7.5 ML. Therefore, surface tension is of opposite trend to the experimental observation, but it accounts for less than 10% of the observed effect and it is neglected.

There must also be a pressure due to the 7% lattice mismatch between the CdS core and the ZnS shell [13]. If epitaxy is maintained, without the incorporation of misfit dislocations, the ZnS lattice must extend and compress the core. To calculate the pressure, we use an isotropic model and continuum elasticity [14]. With spherical symmetry, the displacement u is only radial, such that u_ρ satisfies $\nabla^2 u_\rho = 0$. Therefore, in the core of radius $R < R_0$, $u_{0,\rho}(R) = AR$, while in the shell $u_{1,\rho}(R) = BR + C/R^2$ where the indices 0 and 1 refer to the core and shell, respectively. To determine A, B, and C, the three boundary conditions are zero pressure at the outside radius R_1, $P(R_1) = 0$, continuous pressure at the interface, and the mismatch ε of the lattice constants at R_0 imposes $(u_{0,\rho} - u_{1,\rho}) = \varepsilon R_0$. For CdS and ZnS, $\varepsilon = +0.07$. The pressure as a function of radial position R is then given by

$$P = P_0 \frac{[1 - (R_1/R)^3]}{[1 - (R_1/R_0)^3]}, \quad \text{for } R \geq R_0,$$
$$\text{and} \quad P = P_0 \quad \text{for } R \leq R_0 \tag{1}$$

where the interfacial pressure P_0 is $P_0 = 2E_0E_1\varepsilon[R_1^3/R_0^3 - 1]/\{[2E_1(1-2\nu_0) + E_0(1+\nu_1)]R_1^3/R_0^3 - 2[E_1(1-2\nu_0) - E_0(1-2\nu_1)]\}$.

E and ν are the Young's modulus and Poisson ratios for core (0) and shell (1). The Young's modulus and Poisson ratio are taken from the Reuss-Voigt-Hill average of the cubic lattice elastic constants [15]. For cubic ZnS, experimental data [16] give $E = 86$ GPa and $\nu = 0.32$. Theoretical values for cubic CdS are $E = 68$ GPa and $\nu = 0.34$ [17] while values derived from Wurtzite data [18] are $E = 46$ GPa and $\nu = 0.37$. Results from Eq. (1) are calcu-

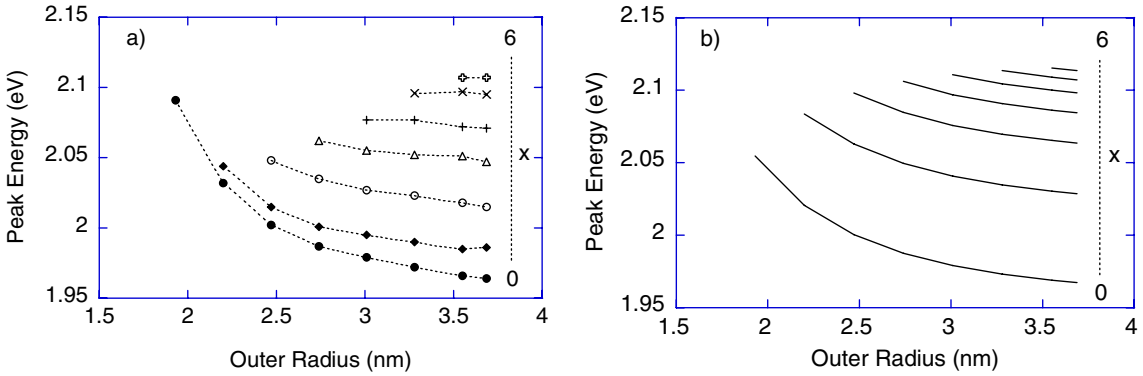

FIG. 3 (color online). Mn^{2+} PL peak as a function of nanoparticle size for $CdS/ZnS_{xML}/Mn/ZnS_{(7.5-x)ML}$. (a) Experimental results. (b) Theoretical results from the elasticity model using a fixed 2.12 eV for the zero-pressure Mn^{2+} emission.

lated with the values given above for ZnS and the average of the two theoretical CdS values. The model shows that the interfacial pressure builds up as the shell thickness increases, saturating to a value that depends on the material properties but not on the initial radius. Using (1), the interfacial pressure saturates to $P_0 = 5.5$ GPa, indeed within the range of the maximum experimental value reported above.

To compare to the experimental data in more detail, one needs the zero-pressure Mn^{2+} emission peak as a reference. In Fig. 3(b), we used a fixed value of 2.12 eV which provides good agreement with increasing shell thickness but with vertical offsets. This is because the Mn^{2+} emission is sensitive to the local environment. In Mn:CdS nanoparticles, the emission is at 2.16 eV [19] compared to 2.12 eV for bulk ZnS. The data show also that the interfacial Mn^{2+} at 2.09 eV is redshifted from both CdS and ZnS bulk values. The peak emission is due to the crystal field, including the metal ions which are the next-nearest neighbors and the local strain. While it is conceivable that future studies could directly analyze the value of the emission peak, this is not possible at the moment.

In this Letter, we propose however that the shift of the emission as shells are built up is simply proportional to the pressure, independently of the local environment. Using the shift instead of the absolute values thus allows a direct comparison between the different positions of Mn^{2+}. Figure 4 shows $\Delta P = \alpha(E(\text{final}) - E(R_1))$ for a given radial position of Mn^{2+} where $E(\text{final})$ is the peak energy when $R_1 = 3.7$ nm (7.5 ML of ZnS) as a function of the nanoparticle size R_1. This is then compared to the theoretical $\Delta P = P(\text{final}) - P(R_1)$ where similarly, $P(\text{final})$ is for $R_1 = 3.7$ nm.

The agreement is excellent with no adjustable parameters. Additional experiments have also been done for Mn^{2+} doped inside CdS cores. The delayed Mn^{2+} phosphorescence peak is observed at 2.162 eV in agreement with previous reports [17] and it redshifts as the ZnS shell is grown. Starting with CdS cores of 3.4 ± 0.4 nm diameter (the size is determined by TEM and the error is the standard deviation on 50 particles) and growing the ZnS shell to a final size of 5.7 ± 0.8 nm diameter, the phosphorescence shifts to 2.031 eV. This corresponds to a core pressure of 4.3 GPa, again in close agreement with the model which gives 4.6 GPa.

The agreement between the Mn^{2+} observations and the continuum elastic model suggests that the model is useful to understand stress in composite structures at the nm scale. For example, for the ZnS shell on CdSe, the lattice mismatch is $\varepsilon = 0.12$. Experimentally, the shell grows smoothly for a couple ML [2], but thick shells are rough [4]. From the expression above, the pressure induced by a hypothetical thick and epitaxial ZnS shell on CdSe would be $\sim$10 GPa. The strain is thus likely to exceed the threshold for creation of misfit dislocations. On the other hand, for CdSe/CdS and CdSe/ZnSe with smaller mismatch, the maximum interfacial pressure remains smaller, possibly allowing unlimited thick shells.

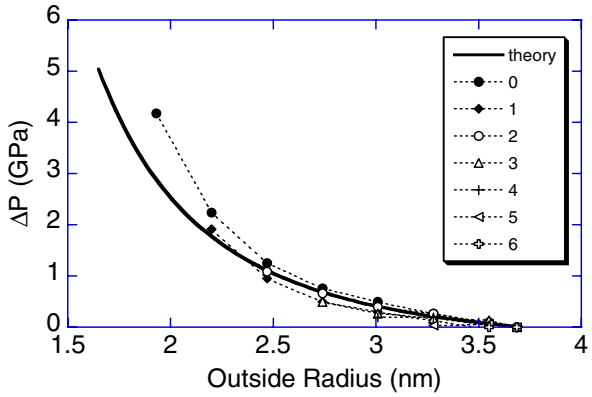

FIG. 4 (color online). Pressure difference between the final shell of 7.5 ML of ZnS and intermediate shell deposition. The symbols are the measured values for Mn^{2+} located at $x = 0$ to 6 ZnS ML from the CdS core as 1 to $7.5 - x$ ML ZnS are deposited. The horizontal error bars are estimated to be <1 ML (0.27 nm) and the vertical error bars are the symbol size. The bold line is the result from the spherical continuum elastic model.

It is also interesting to compare the core/shell pressure to pressures associated with phase transitions in the materials. For bulk ZnS, the zinc-blend–rocksalt transition pressure is 15 GPa, with a hysteresis of 5 GPa [20], therefore well beyond the range discussed here. However, for bulk CdS or CdSe, the conversion from wurtzite–zinc-blend to rocksalt occurs around 2 GPa with a hysteresis width of also ~2 GPa [21]. This is within the regime considered here. With small particles, the hysteresis is broadened, and the pressure of the phase transition is raised [12]. This may explain why CdS/ZnS retains the zinc-blend structure in spite of the high pressures. On the other hand, for larger mismatch, one possible failure of the core/shell growth could be distortions of the core or shell lattice associated with a phase transition of the materials.

The spherical model suggests that epitaxial growth of a fixed shell thickness leads to lower pressures on larger cores and that it should be easier. Yet, it is known that the ZnS shell does not grow better on larger CdSe cores. This discrepancy may arise because the model does not account for crystal anisotropy and the faceting that occurs for larger cores. It should also be noted that the integrated elastic strain energy, for a fixed shell thickness, still grows with core size and that creation of dislocation may simply be energetically favorable.

Lastly, the exciton PL peak of undoped core/shell exhibits a ~0.1 eV blueshift with increasing ZnS layers from 1 to 7.5 ML. This is in rough accordance with the CdS bandgap increase with pressure [19]. However, a determination of the internal pressure based on this observation is not precise since the exciton shift is also related to quantum confinement.

In summary, the emission of Mn^{2+} is sensitive to the local environment but its tuning with shell thickness appears to be an excellent local pressure probe. Using bulk pressure tuning values, the redshift of the Mn^{2+} emission in colloidal CdS/ZnS indicates a pressure increase in excess of 4 GPa as shells are built up. By controlling the Mn^{2+} position and ZnS shell thickness, the radial dependence and magnitude of the pressure were determined. The observations are in good agreement with the simple spherically symmetric elastic continuum model and are attributed to the 7% misfit between the core and the epitaxial shell.

We would like to thank Philippe Monod for the EPR results. This project was partly funded by the Agence Nationale de la Recherche, the Human Frontier Science Program, and the City of Paris.

[1] C. B. Murray, D. J. Norris, and M. G. Bawendi, J. Am. Chem. Soc. **115**, 8706 (1993).
[2] M. A. Hines and P. Guyot-Sionnest, J. Phys. Chem. **100**, 468 (1996).
[3] J. H. Vandermerwe, J. Appl. Phys. **34**, 123 (1963).
[4] Z. H. Yu *et al.*, Nano Lett. **5**, 565 (2005).
[5] G. J. Piermarini *et al.*, J. Appl. Phys. **46**, 2774 (1975).
[6] Y. A. Yang *et al.*, J. Am. Chem. Soc. **128**, 12428 (2006).
[7] Y. C. Cao and J. H. Wang, J. Am. Chem. Soc. **126**, 14336 (2004).
[8] W. W. Yu *et al.*, Chem. Mater. **15**, 2854 (2003).
[9] H. J. Zhou *et al.*, J. Appl. Phys. **99**, 103502 (2006).
[10] R. H. Bube, Phys. Rev. **90**, 70 (1953).
[11] W. Chen *et al.*, J. Lumin. **91**, 139 (2000).
[12] S. H. Tolbert and A. P. Alivisatos, Science **265**, 373 (1994).
[13] *Numerical Data and Functional Relationships in Science and Technology*, edited by K.-H. Hellwege and O. Madelung, Landolt-Börnstein, New Series, group III, Vol. 17 (Springer, Berlin 1982).
[14] A. S. Saada, *Elasticity Theory and Applications* (Pergamon Press, Inc., New York, 1973).
[15] R. Hill, Proc. Phys. Soc. London Sect. A **65**, 349 (1952).
[16] D. Berlincourt, L. R. Shiozawa, and H. Jaffe, Phys. Rev. **129**, 1009 (1963).
[17] E. Deligoz, K. Colakoglu, and Y. Ciftci, Physica. B, Condens. Matter **373B**, 124 (2006).
[18] E. R. Fuller and W. F. Weston, J. Appl. Phys. **45**, 3772 (1974).
[19] G. Counio *et al.*, J. Phys. Chem. **100**, 20021 (1996).
[20] S. Ves *et al.*, Phys. Rev. B **42**, 9113 (1990).
[21] A. L. Edwards and H. G. Drickamer, Phys. Rev. **122**, 1149 (1961).